Catalysis
Science & Technology

Cite this: DOI: 10.1039/c2cy20594g

www.rsc.org/catalysis

PAPER

On the performance of Ag/Al_2O_3 as a HC-SCR catalyst – influence of silver loading, morphology and nature of the reductant

Hannes Kannisto,*[a] Kalle Arve,[b] Torben Pingel,[c] Anders Hellman,[d] Hanna Härelind,[a] Kari Eränen,[b] Eva Olsson,[c] Magnus Skoglundh[a] and Dmitry Yu. Murzin[b]

Received 24th August 2012, Accepted 11th October 2012
DOI: 10.1039/c2cy20594g

This study focuses on the performance of Ag/Al_2O_3 catalysts for hydrocarbon selective catalytic reduction (HC-SCR) of NO_x under lean conditions, using complex hydrocarbons as reductants. The aim is to elucidate the correlation towards the silver loading and morphology, with respect to the nature of the reductant. Ag/Al_2O_3 samples with either 2 or 6 wt% silver loading were prepared, using a sol–gel method including freeze-drying. The catalytic performance of the samples was evaluated by flow reactor experiments, with paraffins, olefins and aromatics of different nature as reductants. The physiochemical properties of the samples were characterized by scanning electron microscopy/energy dispersive X-ray spectroscopy, scanning transmission electron microscopy/high angle annular dark field imaging, X-ray photoelectron spectroscopy and N_2-physisorption. The 2 wt% Ag/Al_2O_3 sample was found to be the most active catalyst in terms of NO_x reduction. However, the results from the activity studies revealed that the decisive factor for high activity at low temperatures is not only connected to the silver loading *per se*. There is also a strong correlation between the silver loading and morphology (*i.e.* the ratio between low- and high-coordinated silver atoms) and the nature of the hydrocarbon, on the activity for NO_x reduction. Calculated reaction rates over the low-coordinated step and high-coordinated terrace sites showed that the morphology of silver has a significant role in the HC-SCR reaction. For applications which include complex hydrocarbons as reductants (*e.g.* diesel), these issues need to be considered when designing highly active catalysts.

Introduction

The negative impact of exhaust emissions on human health and the concerns of global warming have driven environmental legislation towards continuously stricter emission standards for carbon dioxide (CO_2), particulate matter (PM) and nitrogen oxides (NO_x) originating from combustion engines.[1–3] Lean burn and diesel engines have provided a significant fuel economy benefit and thus reduced CO_2 emissions compared to gasoline engines operating under stoichiometric conditions. However, the full global expansion of such engines has been hindered due to the challenges concerning NO_x and PM emissions. Three major techniques to reduce NO_x emissions originating from diesel and lean burn engines have been proposed: NO_x storage and reduction (NSR), selective catalytic reduction with ammonia/urea (NH_3–SCR) or selective catalytic reduction with hydrocarbons (HC-SCR).[4] However, to date none of the above-mentioned systems alone can provide a fully satisfying solution in terms of low-temperature activity under transient conditions, catalyst durability or cost effectiveness for the post-treatment of NO_x in lean exhausts. Nevertheless, a NSR system combined with NH_3–SCR for passenger vehicles has been commercialized[5] and urea systems for heavy duty vehicles have been on the market for several years. Among the different systems, the most elegant technical solution for NO_x reduction would be offered by HC-SCR, even though it is associated with a fuel penalty that depends on the engine-out NO_x levels. Since the pioneering work of Iwamoto *et al.*[6] and Held *et al.*,[7] several catalytic formulations have been proposed,[3,8–16] from which silver supported on alumina has emerged as one of the most promising candidates so far. This catalyst has been proven

[a] *Competence Centre for Catalysis (KCK), Department of Chemical and Biological Engineering, Chalmers University of Technology, SE-41296 Gothenburg, Sweden. E-mail: hannes.kannisto@chalmers.se; Fax: +46 31 16 00 62; Tel: +46 31 772 33 72*
[b] *Laboratory of Industrial Chemistry and Chemical Engineering, Process Chemistry Centre, Åbo Akademi University, Biskopsgatan 8, FIN-20500 Turku/Åbo, Finland*
[c] *Department of Applied Physics, Chalmers University of Technology, SE-412 96 Gothenburg, Sweden*
[d] *Competence Centre for Catalysis (KCK), Department of Applied Physics, Chalmers University of Technology, SE-412 96 Gothenburg, Sweden*

to show high activity for NO_x reduction at elevated temperatures (>300 °C) in the laboratory, engine bench and full-scale tests, using model compounds or diesel with very low sulphur and aromatics content (MK1) as reductants.[11,16,17]

Several research groups have reported that Ag/Al_2O_3 catalysts with a relatively low loading of silver show the highest HC-SCR activity.[9,13,18–31] The optimal silver loading depends on the preparation method of the catalyst as well as on the nature of the hydrocarbon used as the reducing agent. In general, catalysts with approximately 2 wt% silver on alumina have been reported as the most active ones in terms of NO_x reduction.[13,20,26,27] On the other hand, if the silver loading is further increased the undesired total oxidation of the reductant, *i.e.* combustion, becomes the predominant reaction instead of HC-SCR, especially over catalysts prepared by impregnation methods.[9,13,18,24,25,27,29] Catalysts prepared with sol–gel methods are in general more capable of maintaining the selectivity towards NO_x reduction at higher silver loadings than catalysts prepared by impregnation methods.[8,25,32] Nevertheless, for high silver loadings combustion of the hydrocarbon will become favoured also for the sol–gel prepared catalysts and hence the NO_x reduction will be suppressed. Further, high activity is mainly attributed to the formation of small, partially charged silver clusters, acting as the active sites for partial oxidation of the hydrocarbon.[19,28,30,31] However, the above studies have in most cases been performed with alkanes or alkenes as model hydrocarbons.[9,13,18–20,24,25,27–31] The fraction of naphthenes and aromatic hydrocarbons in diesel fuel is more challenging for the Ag/Al_2O_3 catalyst. These hydrocarbons may cause a significant drop in the HC-SCR activity but also shift the NO_x reduction towards higher temperatures.[23,33–35] Using conventional diesel (US06) as the reductant, Houel *et al.*[21–23] reported that a 2 wt% Ag/Al_2O_3 catalyst showed significantly lower NO_x conversion, and also deactivated due to coking at low temperatures (<350 °C), compared to longer alkanes (C_8–C_{12}). Coking was suggested to be due to the aromatics and longer alkenes in the diesel fuel.[23] Arve *et al.*[34] suggested an alternative explanation, taking into account the differences in adsorption kinetics of the different types of hydrocarbons, also supported by a recent study by Demidyuk *et al.*[35]

For alkanes and alkenes, catalysts with higher silver loadings (>4–5 wt%) are commonly reported to show lower activity for HC-SCR, due to combustion of the reductant.[9,13,18,24,25,27,29] Combustion of the reductant has been shown to proceed over larger metallic silver particles, which are formed in higher amounts on catalysts prepared by impregnation methods with silver loadings between or above 2 and 5 wt%.[9,13,18,24,25,27,29] Nevertheless, as the relationship between activity and structure of the silver–alumina catalyst is still under debate, at least for more complex reductants than the model compounds reported,[9,13,18–20,24,25,27–31,33] it is premature to conclude that a catalyst having 2 wt% silver would be the most active HC-SCR catalyst. The relationship between the HC-SCR activity and structure of the reductant molecule, on one hand, and the silver loading, particle size and morphology, on the other hand, has not yet been thoroughly investigated for HC-SCR over Ag/Al_2O_3. Attempts to reveal this connection are scarce,[33] despite the fact that reaction rate dependence on particle size in the size range of 2–20 nm is a very well-known theme in heterogeneous catalysis.[36–42] Therefore, this paper examines the influence of the nature of the reductant, and the effect of silver particle size and morphology in regard to the HC-SCR activity. For this purpose, several paraffinic, olefinic and aromatic reducing agents were used for HC-SCR over silver–alumina catalysts, with 2 or 6 wt% nominal silver loading. The catalysts were characterized in terms of silver particle size and distribution by scanning transmission electron microscopy/high angle annular dark field (STEM/HAADF) imaging. To investigate the influence of the ratio between low-coordinated (step) and high-coordinated (terrace) silver sites on the HC-SCR activity, such ratios were determined by the construction of Wulff shapes of silver particles in the corresponding size range. The dependence of silver particle size and morphology on one hand, and the nature of the reductant on the other hand, for HC-SCR over Ag/Al_2O_3, is elucidated, which is crucial for applications with *e.g.* diesel as a reductant.

Materials and methods

Catalyst preparation

The Ag/Al_2O_3 samples (2 and 6 wt% Ag) were prepared according to the sol–gel method combined with freeze-drying, as previously described by Kannisto *et al.*[25] Silver nitrate (>99.5%; VWR) was dissolved in water (milli-Q) and aluminum isopropoxide (98+%; Aldrich) was slowly added to the $AgNO_3$ solution under vigorous stirring. The resulting slurry was heated to 80 °C and nitric acid (10%; Fluka) was subsequently added drop-wise until a sol was formed. The sol was then kept under stirring for 12 h. Excess solvent was removed under reduced pressure at 30 °C until a gel was formed. The gel was thereafter freeze-dried, heated in air from room temperature (RT) at 2 °C min^{-1} to 600 °C and finally calcined at this temperature for 6 h.

Flow reactor experiments

The activity for lean NO_x reduction (to N_2) was investigated over Ag/Al_2O_3 grains (0.4 g, diameter distribution 250–500 μm) according to the same procedure as described by Arve *et al.*[43] The total flow was 550 ml min^{-1} at RT, corresponding to a space velocity (GHSV) of 60 000 h^{-1}. A temperature range of 150–600 °C with sampling under steady-state conditions (30 min for every 50 °C) was used for the flow reactor experiments. The gas mixture used in the experiments consisted of 500 ppm NO, 6 vol% O_2, 10 vol% CO_2, 350 ppm CO, 12 vol% H_2O, and He as balance. The following hydrocarbons were used, respectively, as reducing agents: propene (333 or 1000 ppm), *n*-octane (375 ppm), cyclohexane (500 ppm), methylcyclohexane (430 ppm), benzene, (500 ppm), toluene (430 ppm) or cumene (isopropylbenzene) (333 ppm). The structures of the different hydrocarbons are shown in Fig. 1. The C/N ratio was kept constant at 6, except for the case of 333 ppm propene (C/N = 2).

The degree of oxidation of the reducing agents in the gas phase and over the support was measured by flowing 6 vol% O_2, 12 vol% H_2O and He as balance through the pure alumina support, under conditions similar to the activity tests.

Catalyst characterisation

N_2-physisorption. The BET surface area of the prepared Ag/Al_2O_3 samples was determined by N_2-physisorption at 77 K

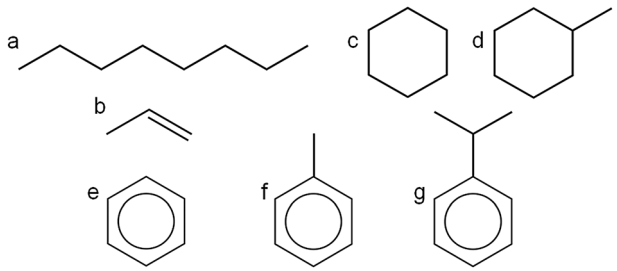

Fig. 1 Structures of the reductants used in this study. (a) *n*-octane, (b) propene, (c) cyclohexane, (d) methylcyclohexane, (e) benzene, (f) toluene and (g) cumene.

Table 1 Physiochemical properties of the Ag/Al_2O_3 samples

	Surface area	Silver loading		STEM/HAADF imaging		
Sample	BET/ $m^2\ g^{-1}$	SEM-EDXS [%]	ICP-SFMS [%]	Particle count	Mean particle size/nm	Median/ nm
2 wt% Ag	174	3.4	2.0	438	4.72	3.33
6 wt% Ag	163	7.7	5.6	1234	5.77	5.38

using a Micromeritics Tristar instrument. All samples were dried at 200 °C in vacuum for 2 h before the analysis. The results are presented in Table 1.

Metal loading. The metal loading of the samples (Table 1) was determined by scanning electron microscopy/energy dispersive X-ray spectroscopy (SEM-EDX), using a Leo Gemini 1530 instrument with a ThermoNORAN Vantage X-ray detector, and also by inductively coupled plasma sector field mass spectrometry (ICP-SFMS).

Scanning transmission electron microscopy. Scanning transmission electron microscopy (STEM) using high angle annular dark field (HAADF) imaging for particle size determination was performed using a FEI Titan-300 transmission electron microscope (TEM), with a probe corrector of spherical aberration (C_s) operating at 300 kV. The samples were prepared by thoroughly crushing the powder catalyst in a mortar and subsequently mixing the powder with ethanol. A drop of the resulting mix was then placed on a carbon sputtered copper grid (3.0 mm, 300 mesh).

X-ray photoelectron spectroscopy. X-ray photoelectron spectroscopy (XPS) measurements were performed to determine the oxidation state of silver in the Ag/Al_2O_3 samples. The measurements were performed using a Perkin-Elmer PHI 5000 C system, equipped with a pre-treatment reactor cell, as described previously by Olsson and Fridell.[44] Pre-treatment was performed for 20 min at 400 °C, in a gas flow of either 2% O_2 or 4% H_2 (Ar bal.). The samples were then cooled in an argon flow, before being transferred to the UHV chamber. XPS spectra were obtained using a monochromated Al K_α X-ray source. Charging of the samples was accounted for by shifting the spectra against the C 1s peak at 284.5 eV.[45]

Silver particle modelling. A Wulff construction was used to determine the equilibrium shape of silver particles between 1 and 20 nm in diameter. Here, the silver particle was modelled as a truncated octahedral by using the surface energy of the (100) and (111) facets for Ag, as calculated by Vitos *et al.*[46] Furthermore, any effect of the support was ignored. In the analysis, the terrace and step atoms, where the latter have a lower coordination number, were counted separately.

Results and discussion

Silver loading

The results from the SEM-EDXS and ICP-SFMS analyses, reporting the silver loadings of the prepared samples, are given in Table 1. As can be seen (ICP-SFMS results), the measured silver loading is somewhat lower than the nominal silver loading (in the precursor solution). The fact that SEM-EDX shows higher silver loading than the nominal value is most likely due to that the analysis is performed rather locally on a relatively small area with a higher silver concentration than the global silver content. Overall the results show that the measured silver loading increases along with the increasing nominal loading and thus it can be concluded that the catalyst preparation route resulted in the desired outcome.

Silver dispersion and particle size. STEM/HAADF imaging was used to determine the particle size and distribution of the silver particles on the alumina support. Micrographs of the prepared Ag/Al_2O_3 catalysts (Fig. 2) are given as representative results, revealing an uneven silver dispersion, with silver particle sizes commonly between 1 and 15 nm (Fig. 3, left). According to the micrographs, the silver particles are apparently located in areas of high silver loading, while other areas of the support are seemingly metal free. It is also noted that some of the silver particles are located directly on the supporting carbon film. Based on the STEM/HAADF results, it can be stated that the mean particle size is 4.72 nm and 5.77 nm for the 2 wt% and 6 wt% sample, respectively (Table 1). However, the median particle size differs more significantly (3.33 nm and 5.38 nm, respectively), which is more important. Furthermore, it is noted that the number of observed particles increases virtually 1 : 1 with the silver loading. Such a good correlation between the amount of particles and the silver loading is unexpected. However, the correlation should be used with caution, as only two points of reference are used. Nevertheless this result is

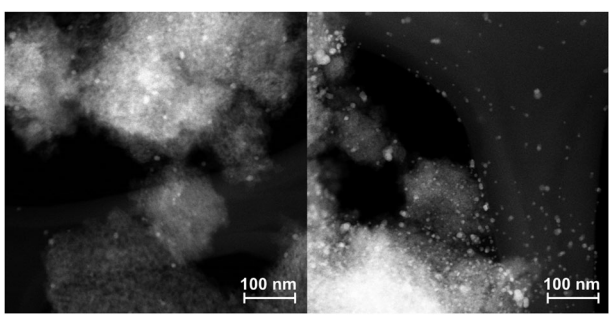

Fig. 2 STEM/HAADF micrographs of the 2 wt% (left) and 6 wt% (right) Ag/Al_2O_3 samples.

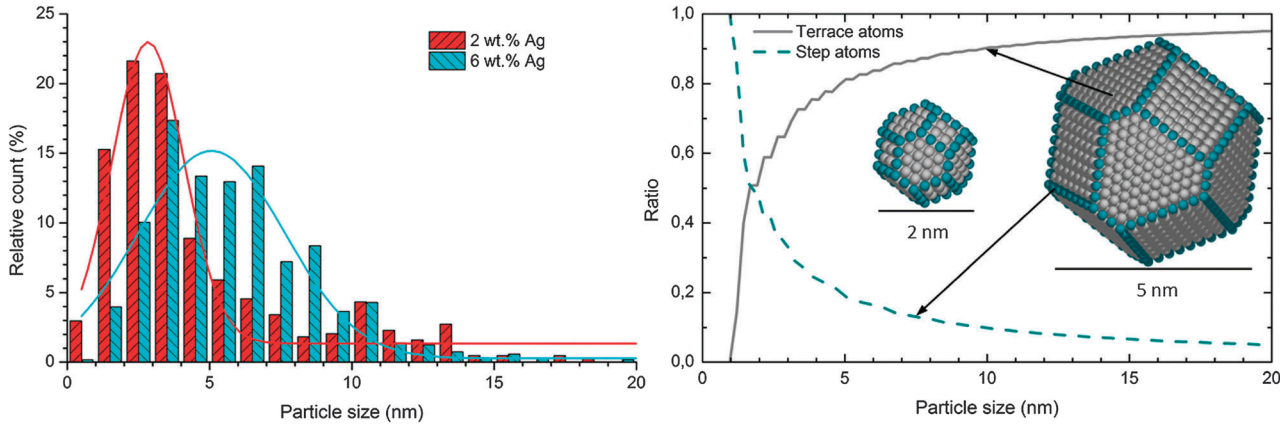

Fig. 3 (left) Particle size (diameter) histograms of the 2 wt% sample and 6 wt% sample, with fitted Gauss functions (lines). The particle count is stated in Table 1. (right) Step *vs*. terrace atomic ratio as a function of silver particle size. Constructed Wulff shapes for 2 and 5 nm silver particles. Step atoms are highlighted.

logical, as the mean particle size is only slightly higher and also the particle size distribution is somewhat broader for the 6 wt% sample, as shown in Fig. 3 (left). Further, it is also noted that several silver particles show polyhedral shapes, indicating that they are close to thermodynamic equilibrium.

According to Fig. 3 the most abundant silver particles are in the size range of 2–3 nm for the 2 wt% sample, and around 5 nm for the 6 wt% sample. This is important, as the ratio between step and terrace atoms is different for these particle sizes (Fig. 3, right). For the smallest silver particles (*i.e.* less than 1 nm in diameter) there are no terrace atoms. For particles between 1 and 2 nm, the ratio between terrace and step atoms increases steeply with increasing particle size, reaching 1 : 1 for particles of 2 nm in diameter. As the ratio increases with 1/radius, particles larger than 5 nm contain only a small fraction (below 20%) of step atoms. According to the STEM/HAADF analysis, several silver particles in the analyzed samples show polyhedral shapes, similar to the constructed Wulff shapes. Thus, it is reasonable to assume that the ratio between step and terrace silver atoms shows a similar dependence on particle size as for the constructed Ag particles. Further, it is also plausible to conclude that the 2 wt% sample contains a considerably higher fraction of low-coordinated silver atoms in comparison with the 6 wt% sample.

Oxidation state of silver

The oxidation state of silver is an important factor to consider, as many reports have suggested (partially) oxidized silver species as the active site for HC-SCR.[13,18,28–31,47,48] It is very likely that partially oxidized silver species are present in the samples, as silver interacts with the alumina support. This especially concerns the 2 wt% sample, as the smaller size of the silver particles allows for a stronger interaction with the support. The XPS measurements after oxidative and reductive pre-treatment (Table 2) show that silver is (partially) oxidized in both samples. The differences between the samples are small, however the results indicate that the relative amount of small silver clusters is higher in the 2 wt% sample. This is supported by the shift towards higher binding energies (BE) for the 2 wt% sample, compared to the 6 wt% sample.[25,49] As

Table 2 Binding energies of $Ag3d_{5/2}$ for the pre-treated samples

Sample	BE/eV	
2 wt% Ag	368.1	367.6
6 wt%	367.9	367.5
Pre-treatment[a]	Oxidation	Reduction

[a] 20 min at 400 °C in 2% O_2 or 4% H_2.

reported by Guo *et al.*,[49] small silver clusters on alumina shift towards higher BE when treated with oxygen. Furthermore, during the HC-SCR reaction the surface of the catalyst is continuously reduced and re-oxidized, as different gas phase species adsorbs and reacts, making it difficult to determine the exact oxidation state of silver. Nevertheless, recent studies[50] have shown that the well-documented Brønsted–Evans–Polanyi (BEP) relation for metals also applies for transition metal oxides. This indicates that the arguments for different activities on the steps and terraces also hold for (partially) oxidized Ag particles.

Activity tests

The aim of this work is to study the influence of the silver loading and morphology, and the nature of the hydrocarbon as a reductant in the NO_x reduction over Ag/Al_2O_3 catalysts. Fig. 4 show the results from the flow reactor experiments over the Ag/Al_2O_3 samples using a variety of alkanes, cycloalkanes and aromatics, *i.e.* *n*-octane, cyclohexane, methylcyclohexane, benzene, toluene and cumene (isopropylbenzene). In general, the NO_x reduction decreases with increased silver loading as the rate of the competitive total oxidation of the hydrocarbon increases.[9,13,18,24,25,27,29] Using *n*-octane as the reductant the NO_x reduction starts approximately at the same temperature over the two catalysts, however for the sample with lower silver loading the NO_x reduction is clearly higher and proceeds over a considerably broader temperature range than for the 6 wt% sample. Changing the nature of the reducing agent from linear alkane to cyclic alkanes and aromatics results in lower maximum NO_x reduction and a shift of the NO_x reduction starts towards higher temperature in the following order: methylcyclohexane < cumene < cyclohexane < toluene < benzene for both catalysts. Previously, Arve *et al.*[33]

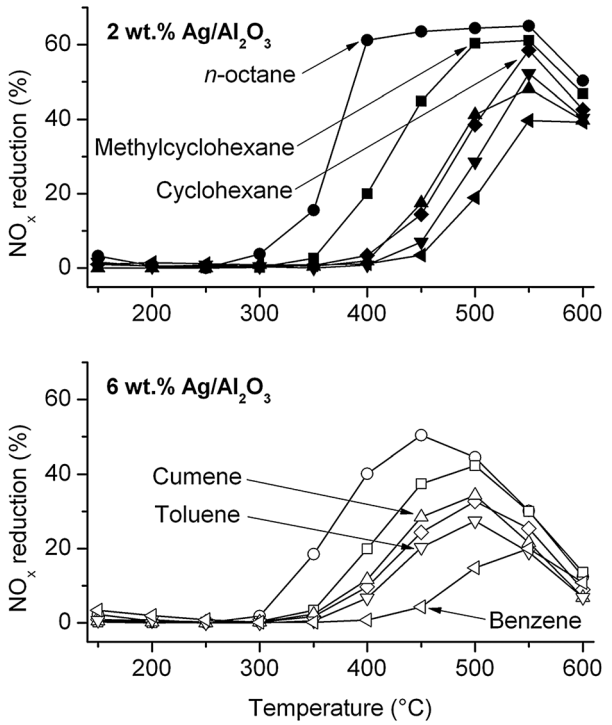

Fig. 4 NO_x reduction *vs.* temperature over the 2 wt% (closed markers) and 6 wt% (open markers) catalyst, using *n*-octane (●), cyclohexane (◆), methylcyclohexane (■), benzene (◀), toluene (▼) or cumene (▲) as reductants. Gas feed: 500 ppm NO, 6 vol% O_2, 10 vol% CO_2, 350 ppm CO, 12 vol% H_2O, He bal. C/N = 6. Total flow: 500 ml min^{-1}. GHSV = 60 000 h^{-1}.

have shown similar results, comparing the effects of *n*-octane, methylcyclohexane and toluene as reductants over a 2 wt% Ag/Al_2O_3 catalyst prepared by wet impregnation. Additionally, the results in Fig. 4 show that the NO_x reduction starts at lower temperatures, as an alkyl group is added to the aliphatic as well as the aromatic ring. Further, the NO_x reduction increases with the complexity of the alkyl group. Most likely, the secondary carbon in the propyl group of cumene has an influence in this matter, as it stabilizes the alkyl group and weakens the C–C bond to the aromatic ring, which may be of importance for the NO_x reduction.[32] The cycloparaffinic hydrocarbons show higher NO_x reduction than the corresponding aromatic hydrocarbons, *cf.* cyclohexane *vs.* benzene and methylcyclohexane *vs.* toluene in Fig. 4. This is due to the lower reactivity of the aromatics over the Ag/Al_2O_3 catalyst. This means that the reaction between adsorbed NO_x and partially oxidized hydrocarbon species, which has been shown to be an important step in the reaction mechanism,[10,17] is shifted towards higher temperature as compared to the cycloparaffins. Thus, for a given temperature, the amount of available partially oxidized hydrocarbon species is higher for the cyclic paraffins than for the corresponding aromatics. The aromatic ring is very stable, thereby resistant towards partial oxidation, as the H–C bond strength is much higher compared to *e.g.* cyclic paraffins (see Table 3). However, as shown in Fig. 4, the reactivity of the aromatic compounds as well as the cyclic paraffinic compounds increases by the addition of an alkyl group to the carbon ring. Compared to benzene, toluene and particularly cumene show higher NO_x reduction over both catalysts.

Table 3 Bond strengths for different hydrocarbons[51,52]

Hydrocarbon	Bond	Bond energy/kJ mol^{-1}
Propene	H–CH_2CHCH_2	361.9 ± 8.8
Propane	H–*n*-C_3H_7	423.3 ± 2.1
	H–*i*-C_3H_7	409.1 ± 2.0
Benzene	H–C_6H_5	473.1 ± 3.0
Toluene	H–$CH_2C_6H_5$	375.7 ± 1.7
	CH_3–C_6H_5	317.1 ± 6.3
Cumene	H–$C(CH_3)_2C_6H_5$	353.1 ± 6.3
	CH_3–$CH(CH_3)C_6H_5$	312.1 ± 6.3
Cyclohexane	H–cyclohexyl	399.6 ± 4
Methylcyclohexane[a]	H–$CH_2C_6H_{11}$	415–435

[a] Value approximately 40–60 kJ mol^{-1} higher than the corresponding bond for toluene due to less delocalization.[51]

Methylcyclohexane shows accordingly higher NO_x reduction than cyclohexane. For toluene, the NO_x reduction over the 2 wt% catalyst is approximately 10% at 450 °C, whereas the reduction over the 6 wt% sample, using the same reductant, is approximately 20%. Furthermore, for cumene at 450 °C, the activity follows the same trend as for toluene.

The most likely explanation for the higher activity of the alkylated compounds is that the abstraction of a hydrogen in the alkyl group, or the abstraction of the entire alkyl group, is facilitated compared to abstraction of the first hydrogen in the paraffinic or aromatic carbon ring (see Table 2). Considering the abstraction of a methyl group from toluene, Keshavaraja *et al.*[53] reported NO_x reduction around or below 10% at 450 °C over Ag/Al_2O_3 with methane as the reductant (C/N = 8). However, the space velocity was only 9000 h^{-1}, which corresponds to almost seven times higher contact time compared to the present study. Although the methyl group would be more active for HC-SCR than methane, assuming that the higher activity of the alkylated hydrocarbons solely could be ascribed to reduction of NO_x by the alkyl group can be ruled out, the C/N ratio for methyl alone would only be 0.86. In the case of cumene the possible role of reduction by the alkyl group is more relevant, as a propyl group may be cleaved from cumene. Fig. 5 shows the NO_x reduction over both the 2 wt% and 6 wt% samples with propene as the reductant. As can be seen, for C/N = 6 the NO_x reduction at 450 °C (Fig. 5) exceeds the activity recorded for cumene (Fig. 4). However, the C/N ratio for propyl alone would only be 2. At such low C/N ratio the NO_x reduction over the 6 wt% sample is only 17.5%, as can be seen from Fig. 5, significantly lower than for cumene as the reductant. Considering the reducing potential of the cleaved hydrogen or alkyl group, it is not likely that the higher activity of the alkylated compounds can be ascribed to reduction entirely by the cleaved group. A more likely explanation of the higher activity of the alkylated compounds involves the entire molecule. By the abstraction of the first hydrogen or the alkyl group, the entire molecule is activated and consequently prone to partial oxidation and further reaction with NO_x.

Oxidation over the support may also be a factor that could influence the reactivity of the reductant. To determine the oxidation of the reductant over the support (not shown), selected reductants (*n*-octane, benzene and toluene) together with 6 vol% O_2, 12 vol% H_2O and He as balance were fed over

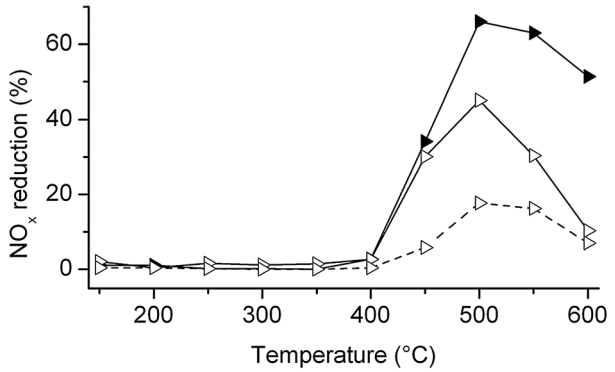

Fig. 5 NO_x conversion *vs.* temperature over the 2 wt% (closed markers) and 6 wt% (open markers) catalysts, using propene as the reductant. Gas feed: 500 ppm NO, 6 vol% O_2, 10 vol% CO_2, 350 ppm CO, 12 vol% H_2O, He bal. C/N = 6 (line) or 2 (dashed). Total flow: 500 ml min^{-1}. GHSV = 60 000 h^{-1}.

pure alumina, prepared by the same sol–gel method as the Ag/Al_2O_3 samples. The measurements were performed in the same temperature range and with the corresponding amount of hydrocarbons as in the activity tests reported above. The oxidation over alumina starts at 400 °C for all reductants and then increases with temperature. As expected, *n*-octane is the most easily oxidized hydrocarbon over alumina, while benzene shows the lowest degree of oxidation. The degree of oxidation also increases with addition of an alkyl group, but nevertheless, the oxidation over the alumina is much lower than the oxidation over the Ag/Al_2O_3 samples during the HC-SCR reaction. As a comparison, the maximum total oxidation of toluene is *ca.* 85% over both catalysts at 600 °C, while only 14% over pure alumina. The other tested hydrocarbons show similar results. As the activity for oxidation of the different hydrocarbons is similar, it cannot be concluded that the higher NO_x reduction measured using alkylated cycloparaffins and alkylated aromatics is due to increased oxidation over the support, and/or possibly gas phase oxidation. Furthermore, the oxidation of hydrocarbons clearly starts at lower temperature over the 6 wt% sample, at 350 °C for both toluene and benzene as reductants. Over the 2 wt% sample, the oxidation starts at 400 °C for toluene and 450 °C for benzene, respectively. This clearly shows that toluene with its alkyl group is more easily oxidized than benzene. The trend is similar comparing methylcyclohexane and cyclohexane.

Fouling of Ag/Al_2O_3 samples

Visual inspection of the samples after the activity tests showed, in most cases, traces of black deposits at the front of the samples. This may indicate fouling of the silver alumina catalysts by coking. According to Houel *et al.*,[23] coking of the catalyst is due to aromatics and long alkanes. Nevertheless, visual inspection of the 2 wt% catalyst after the experiment with benzene showed a purely white catalyst with no traces of deposits on the surface. However, after experiments with the alkylated aromatic compounds, toluene and cumene, traces of carbon deposition similar to the paraffins were seen. Although the precision and reliability of visual inspection may be questioned, the differences between the reductants in terms of deposits are very clear. This indicates that the aromatic structure of the hydrocarbon is not necessarily the reason for coking of the catalyst. Rather, there is a possibility that the paraffinic and olefinic structures promote the formation of carbon deposits.

Silver particle size *vs.* type of reductant

The results from the flow reactor experiments (Fig. 4) show that the reduction of NO_x starts at lower temperatures as the silver content of the catalyst increases when alkylated aromatics and paraffins are used as reductants. Moreover, neither cleaved methyl or propyl groups, nor the oxidation over the alumina support can sufficiently explain the differences in NO_x reduction over different catalysts, as discussed above. Therefore, we suggest that the NO_x reduction is not only connected to a certain optimised silver loading, but also to the nature of the reductant. In addition, the results in Fig. 4 provide support for the hypothesis presented by Arve *et al.*[34] that the reduction rate is not only a function of the hydrocarbon concentration but also of its chain length, spatial arrangement and presence of functional groups. A similar concept has also been suggested by Kannisto *et al.*,[25] *i.e.* that a balance between oxidation sites (*e.g.* large silver particles) for activation of the hydrocarbon and reduction sites for the subsequent formation of N_2 is required for high NO_x reduction. This balance was also suggested to be dependent on the reducing agent.[25] Recently, Härelind *et al.*[32] have studied the influence of the C–C bond order for ethane, ethene and ethyne on the reduction of NO_x over 2 and 6 wt% Ag/Al_2O_3 catalysts. The highest activity was observed for C_2H_2, which was concluded to be due to a stronger interaction between ethyne and the catalyst surface. This was owing to higher sticking probability, more easily accessible π-electrons and a more favourable orientation of the molecule, as compared to ethane and ethene.[32]

As the rate of any catalytic reaction depends on the rate constant and reactant coverage, the following conclusion can be made for the reaction in the present study: as the NO_x reduction over the catalysts used in this study strongly depends on the nature of the reducing agent, the activity is connected either to changes in the rate constant or in the coverage of the active sites by the different species. Burch *et al.*[54] and Arve *et al.*[55] have suggested that the HC-SCR mechanism includes dissociative chemisorption of the hydrocarbon, with the breaking of a C–H bond as the rate determining step.[54,55] Thus, it is important to consider bond strengths and structure of the reducing agent used for the HC-SCR reaction. It is apparent that as the bond strengths are different, the activation energies will differ as well according to the linear free energy relationship.[56] This in turn affects the rate of the NO_x reduction. On the other hand, it is clear that the coverage of the reducing agent also has an effect on the rate. The reductant coverage depends on the concentration and nature of the adsorbing molecule, including accessible π-electrons, molecular orientation and sticking probability, as well as on the size and structure of the active metal particles. As the number of larger silver particles increases with the increasing silver loading as shown by the STEM/HAADF analysis (Fig. 2 and 3), this should also be taken into account when trying to understand such a complex system like HC-SCR

over Ag/Al_2O_3. The difference in size distribution of the silver particles is likely to be one of the reasons for the diverse activities over the different samples, even though *ex situ* characterization is not sufficient to provide a conclusive proof for this suggestion. Especially in the case of alkylated aromatic hydrocarbons, it may be of crucial importance to have different silver species as the nature and geometry of these reducing agents also vary compared to the paraffinic ones.

As reported by van Santen,[42] catalytic reactions including activation of π-bonds are very structure sensitive, as the activation of π-bonds requires the presence of several reaction sites including both step- and terrace atoms. Such sites are not present on transition metal particles smaller than 2 nm, according to van Santen.[42] The STEM/HAADF analysis shows that the 6 wt% sample contains a considerably higher number of silver particles in the 5–10 nm range, compared to the 2 wt% sample. As the same types and concentrations of hydrocarbons were used over both samples, the differences in activity cannot be attributed to the different bond energies in the hydrocarbons or varying availability of reductants due to concentration changes in the feed gas. Thus, a reasonable explanation is that the coverage of the hydrocarbon species depends on the size of the metal nanoparticles[34–40] and that the overall activity in the HC-SCR of NO_x over Ag/Al_2O_3 depends both on the C–H bond energy in the hydrocarbon as well as on the coverage of the hydrocarbon, which is a function of the nature of the hydrocarbon and the size of the silver particles. For alkanes, Burch *et al.*[54] have proposed that the SCR mechanism includes dissociative chemisorption, involving breaking of a C–H bond by abstraction of hydrogen by adsorbed oxygen. Arve *et al.*[55] proposed a simplified reaction mechanism where C_xH_{2x+1}* species are formed in the reaction between adsorbed alkanes and oxygen, which further reacts with either oxygen to form CO_2, or with adsorbed NO species to proceed through the HC-SCR reaction, resulting in the formation of N_2. Based on these proposed reaction mechanisms it is reasonable to assume that the observations made in the present study are due to the varying amount of adsorbed active hydrocarbon species on the two catalysts. The reason for the variation is, besides the nature of the reducing agent, the difference in morphology, particle size distribution of the silver and number of silver particles and thereby active sites, resulting in different adsorption modes (*e.g.* sticking probability, accessible π-electrons and molecular orientation) of the reducing agents over the different samples. Further, once the hydrocarbon is activated, the HC-SCR path in the mechanism becomes available.

Based on this reasoning, the following scenario is suggested for the present case with cycloparaffinic and aromatic compounds: To activate the hydrocarbon for HC-SCR, partial oxidation of the hydrocarbon is required, where opening of the carbon ring is a prerequisite. This naturally applies for benzene and cyclohexane, however also for the alkylated compounds, as the cleaved alkyl groups not alone have sufficient reduction potential to explain the increased activity for the alkylated cyclic and aromatic hydrocarbons, over the 6 wt% sample. The opening of the carbon ring most likely occurs at special sites on the silver particles, including both terrace and step atoms.[34–40] However, although the smaller particles in the 2 wt% sample provide a higher fraction of step sites, compared to the larger particles in the 6 wt% sample (Fig. 3, right), the HC-SCR activity is lower at 400–450 °C (Fig. 4). This is likely due to the lower number of sites on the 2 wt% sample, but may also be due to HC-poisoning of the small particles at these temperatures. As the relative proportion of low-coordinated and high-coordinated surface atoms depends on the particle size, the fraction of step and terrace atoms in the 2 and 6 wt% samples was calculated assuming truncated octahedral particle morphology and using particle sizes of 2 and 5 nm, as shown in Fig. 3. Further, all silver sites are assumed to be available for the reaction. Thus, the following equations for the observed activity (TOF_{obs}) can be written for both catalysts:

$$\text{2 wt\% sample: } TOF_{obs} = a \times TOF_{step} + (1 - a) \times TOF_{terrace} \quad (1)$$

$$\text{6 wt\% sample: } TOF_{obs} = b \times TOF_{step} + (1 - b) \times TOF_{terrace} \quad (2)$$

where $a = 0.5$ and $b = 0.2$ based on the step *vs.* terrace atomic ratio shown in Fig. 3. Partial oxidation of silver was not considered. However, since the BEP-relation also applies for transition metal oxides,[50] it can be assumed that the arguments raised above also hold for (partially) oxidized silver. In Table 4 the results from the calculations are presented for cumene as the reductant, which clearly demonstrates varying activities in terms of global NO_x reduction over the 2 and 6 wt% samples as a function of temperature.

Based on the results shown in Table 4, it can be concluded that at 400 °C the 6 wt% sample shows higher activity both in NO_x reduction and hydrocarbon oxidation. Furthermore, the high coordinated terrace sites are almost four times more active in cumene oxidation than the low-coordinated step sites. In addition, at 400 °C the NO to N_2 is practically only taking place over the 6 wt% sample on the terrace sites. As the temperature increases to 450 °C it is observed that the step

Table 4 Global NO_x reduction and HC (cumene) oxidation over low- and high-coordinated silver surface sites

Catalyst	NO_x reduction [%]	TOF_{obs}[a]/ s^{-1}	TOF_{step}[a]/ s^{-1}	$TOF_{terrace}$[a]/ s^{-1}	ΔE_{app}/ kJ mol^{-1}
Temperature 400 °C					
2 wt%	1.9	0.0002	—	0.0015	—
6 wt%	11.7	0.0010			
	HC oxidation [%]				
2 wt%	16.2	0.0012	0.0005	0.0019	7.1
6 wt%	27.2	0.0016			
Temperature 450 °C					
2 wt%	17.5	0.0017	0.00053	0.0029	10.2
6 wt%	28.5	0.0024			
	HC oxidation [%]				
2 wt%	43.7	0.0029	0.0017	0.0041	5.3
6 wt%	65.1	0.0036			
Temperature 500 °C					
2 wt%	41.2	0.0044	0.0066	0.0022	7.1
6 wt%	34.3	0.0031			
	HC oxidation [%]				
2 wt%	83.1	0.0059	0.0069	0.0049	2.2
6 wt%	89.8	0.0053			

[a] All silver sites are assumed to be available for the reaction.

sites also become active in NO reduction. However, the highly coordinated terrace sites are still the predominant reduction sites. On the other hand, the TOF values calculated on step and terrace sites clearly show that by increasing the temperature, the activity over the low-coordinated step sites for cumene oxidation increases rapidly, showing higher TOF than the terrace sites at 500 °C. However, the corresponding calculations for the other reducing agents used in this study show that the activity for oxidation of the different aromatic hydrocarbons over the prepared catalysts remains close to each other. Such experimental observations indicate that the low-coordinated step sites could be possible sites for oxygen adsorption and dissociation leading to hydrocarbon oxidation or they could be the sites responsible for breaking of the C–H (or C–C) bond, which is an important step in the mechanism.[49,50]

As the temperature is further increased to 500 °C, some interesting observations are made. First, at 500 °C the 2 wt% catalyst becomes more active in terms of global NO_x reduction than the 6 wt% sample. Second, as can be seen from Table 4, at 500 °C the low-coordinated sites are more active in terms of global NO_x reduction and HC oxidation compared to the high-coordinated sites. At 400 and 450 °C the opposite behaviour is observed. Thus, it can be concluded that the apparent activation energies for the global NO_x reduction reaction over the step and terrace sites change as a function of temperature. Therefore, the difference in apparent activation energy between the two differently coordinated sites was calculated making the assumption that the sticking coefficients for both types of sites are equal to one (Table 4). It is observed that at 450 °C the apparent activation energy over the terrace sites for global NO_x reduction is roughly 10 kJ mol^{-1} lower than over the step sites. On the other hand, for HC oxidation the apparent activation energy is approximately 5.3 kJ mol^{-1} higher over the step sites than over the terrace sites. At 500 °C the difference in the apparent activation energy for HC oxidation is lower on the low-coordinated sites. For the global NO_x reduction the apparent activation energy over the step sites is calculated to be 7.1 kJ mol^{-1} lower compared to the terrace sites, making these sites more active for the SCR reaction. Such differences in apparent activation energies support the assumption presented in this paper, that HC-SCR over the Ag/Al_2O_3 catalyst is a clearly structure sensitive reaction. Furthermore, the numerical analysis helps in understanding the properties of the silver catalysts during HC-SCR. It can be concluded that for oxidation of hydrocarbons the morphology of the silver particles supported on alumina does not play a significant role. This is in contrast to NO_x reduction, where low-coordinated sites are needed for high temperature activity, while high-coordinated sites are important for the low temperature activity. This indicates that silver catalysts with a bimodal silver distribution are required for catalysts operating within a broad temperature range, when using complex reductants such as diesel fuel.

Conclusions

The activity for lean NO_x reduction by hydrocarbons over Ag/Al_2O_3 is highly dependent on the nature of the reducing agent. For alkylated cyclic paraffins and alkylated aromatics a higher NO_x reduction is observed compared to the corresponding non-alkylated cyclic or aromatic hydrocarbons. Moreover, the activity increases with increasing chain length of the alkyl group. The NO_x reduction is dependent on the partial oxidation of the reductant, which in turn is dependent on the C–H (or C–C) bond strength, accessibility of π-electrons, molecular orientation and sticking probability of the hydrocarbon reductant, *i.e.* the nature of the hydrocarbon.

In addition, it was found that the NO_x reduction over the catalyst is not only dependent on the nature of the reducing agent, but also on the silver loading and morphology. For alkylated cycloparaffinic and alkylated aromatic hydrocarbons, the NO_x reduction is clearly higher at temperatures below 500 °C for the 6 wt% Ag/Al_2O_3 sample, than for the 2 wt% sample. The results from the STEM/HAADF imaging show that the 6 wt% sample contains a higher total number of silver particles than the 2 wt% sample, and also a much higher fraction of silver particles in the 5 nm range. Further, the 2 wt% sample contains a higher fraction of small, 2–3 nm particles. Together with the observed differences in NO_x reduction below 500 °C, this strongly indicates that the HC-SCR reaction is dependent on the ratio between low- and high-coordinated silver atoms. Moreover, the calculated rates over the low- and high-coordinated sites for NO_x reduction and HC oxidation manifests that the overall NO_x reduction rate is a function of the nature of the reducing agent and the silver morphology. Thus, for rational catalyst design resulting in an optimal HC-SCR activity within a broad temperature range, these parameters need to be optimized.

Acknowledgements

Tor Lauren at the Department of Inorganic Chemistry, Åbo Akademi, is greatly acknowledged for the aid with the SEM-EDXS analysis. Fredrik Gunnarsson at the Competence Centre for Catalysis (KCK), Chalmers University of Technology, is acknowledged for the BET surface area measurements. Part of this work (Hannes Kannisto) is financially supported by MISTRA (The Foundation for Strategic Environmental Research) and the Swedish Road Administration and has been performed as part of the MISTRA programme E4 (Energy Efficient Reduction of Exhaust Emissions from Vehicles), within KCK. KCK is financially supported by Chalmers University of Technology, the Swedish Energy Agency and the member companies: AB Volvo, Volvo Car Corporation, Scania CV AB, Haldor Topsøe A/S and ECAPS AB. This work is also part of the activities at the Åbo Akademi Process Chemistry Centre within the Finnish Centre of Excellence Programme (2006–2011). Eva Olsson thankfully acknowledges the Knut and Alice Wallenberg Foundation, Dnr KAW 2003.0141, and The Swedish Research Council (822-2005-2519) for financial support.

Notes and references

1 USDoT, http://www.bts.gov/publications/national_transportation_statistics/html/table_04_32b.html, Accessed 2010-07-12, 2008.
2 DieselNet, http://www.dieselnet.com/standards/, Accessed 2010-07-12.
3 A. Fritz and V. Pitchon, *Appl. Catal., B*, 1997, **13**, 1–25.

4 R. Burch, *Catal. Rev. Sci. Eng.*, 2004, **46**, 271–333.
5 M. Weibel, N. Waldbusser, R. Wunsch, D. Chatterjee, B. Bandl-Konrad and B. Krutzsch, *Top. Catal.*, 2009, **52**, 1702–1708.
6 M. Iwamoto, H. Yahiro, Y. Yuu, S. Shundo and N. Mizuno, *Shokubai*, 1990, **32**, 430–433.
7 W. Held, A. Koenig, T. Richter and L. Puppe, *SAE Paper*, 1990, **SP–810**, 13–20.
8 A. Martínez-Arias, M. Fernández-García, A. Iglesias-Juez, J. A. Anderson, J. C. Conesa and J. Soria, *Appl. Catal., B*, 2000, **28**, 29–41.
9 K. A. Bethke and H. H. Kung, *J. Catal.*, 1997, **172**, 93–102.
10 R. Burch, J. P. Breen and F. C. Meunier, *Appl. Catal., B*, 2002, **39**, 283–303.
11 F. Klingstedt, K. Eränen, L. E. Lindfors, S. Andersson, L. Cider, C. Landberg, E. Jobson, L. Eriksson, T. Ilkenhans and D. Webster, *Top. Catal.*, 2004, **30–31**, 27–30.
12 T. Miyadera, *Appl. Catal., B*, 1993, **2**, 199–205.
13 K. Shimizu, J. Shibata, H. Yoshida, A. Satsuma and T. Hattori, *Appl. Catal., B*, 2001, **30**, 151–162.
14 K. Sato, T. Yoshinari, Y. Kintaichi, M. Haneda and H. Hamada, *Appl. Catal., B*, 2003, **44**, 67–78.
15 R. Burch and P. J. Millington, *Catal. Today*, 1996, **29**, 37–42.
16 K. Eränen, L. E. Lindfors, F. Klingstedt and D. Y. Murzin, *J. Catal.*, 2003, **219**, 25–40.
17 K. Eränen, F. Klingstedt, K. Arve, L. E. Lindfors and D. Y. Murzin, *J. Catal.*, 2004, **227**, 328–343.
18 N. Bogdanchikova, F. C. Meunier, M. Avalos-Borja, J. P. Breen and A. Pestryakov, *Appl. Catal., B*, 2002, **36**, 287–297.
19 J. P. Breen and R. Burch, *Top. Catal.*, 2006, **39**, 53–58.
20 T. E. Hoost, R. J. Kudla, K. M. Collins and M. S. Chattha, *Appl. Catal., B*, 1997, **13**, 59–67.
21 V. Houel, D. James, P. Millington, S. Pollington, S. Poulston, R. Rajaram and R. Torbati, *J. Catal.*, 2005, **230**, 150–157.
22 V. Houel, P. Millington, R. Rajaram and A. Tsolakis, *Appl. Catal., B*, 2007, **77**, 29–34.
23 V. Houel, P. Millington, R. Rajaram and A. Tsolakis, *Appl. Catal., B*, 2007, **73**, 203–207.
24 A. Iglesias-Juez, M. Fernandez-Garcia, A. Martinez-Arias, Z. Schay, Z. Koppany, A. B. Hungria, A. Fuerte, J. A. Anderson, J. C. Conesa and J. Soria, *Top. Catal.*, 2004, **30–31**, 65–70.
25 H. Kannisto, H. H. Ingelsten and M. Skoglundh, *J. Mol. Catal. A: Chem.*, 2009, **302**, 86–96.
26 L. E. Lindfors, K. Eränen, F. Klingstedt and D. Y. Murzin, *Top. Catal.*, 2004, **28**, 185–189.
27 F. C. Meunier, J. P. Breen, V. Zuzaniuk, M. Olsson and J. R. H. Ross, *J. Catal.*, 1999, **187**, 493–505.
28 A. Satsuma, J. Shibata, K. Shimizu and T. Hattori, *Catal. Surv. Asia*, 2005, **9**, 75–85.
29 X. She and M. Flytzani-Stephanopoulos, *J. Catal.*, 2006, **237**, 79–93.
30 J. Shibata, Y. Takada, A. Shichi, S. Satokawa, A. Satsuma and T. Hattori, *J. Catal.*, 2004, **222**, 368–376.
31 K. Shimizu, M. Tsuzuki, K. Kato, S. Yokota, K. Okumura and A. Satsuma, *J. Phys. Chem. C*, 2007, **111**, 950–959.
32 H. Härelind, F. Gunnarsson, S. M. S. Vaghefi, M. Skoglundh and P.-A. Carlsson, *ACS Catal.*, 2012, **2**, 1615–1623.
33 K. Arve, H. Backman, F. Klingstedt, K. Eränen and D. Y. Murzin, *Appl. Catal., B*, 2007, **70**, 65–72.
34 K. Arve, J. R. H. Carucci, K. Eränen, A. Aho and D. Y. Murzin, *Appl. Catal., B*, 2009, **90**, 603–612.
35 V. Demidyuk, C. Hardacre, R. Burch, A. Mhadeshwar, D. Norton and D. Hancu, *Catal. Today*, 2011, **164**, 515–519.
36 D. Y. Murzin, *Langmuir*, 2009, **26**, 4854–4859.
37 A. T. Bell, *Science*, 2003, **299**, 1688–1691.
38 R. Schlögl and S. B. A. Hamid, *Angew. Chem., Int. Ed.*, 2004, **43**, 1628–1637.
39 R. Narayanan and M. El-Sayed, *Top. Catal.*, 2008, **47**, 15–21.
40 C. R. Henry, *Appl. Surf. Sci.*, 2000, **164**, 252–259.
41 J. R. Rostrup-Nielsen, *J. Catal.*, 1972, **27**, 343–356.
42 R. A. Van Santen, *Acc. Chem. Res.*, 2008, **42**, 57–66.
43 K. Arve, L. Capek, F. Klingstedt, K. Eränen, L. E. Lindfors, D. Y. Murzin, J. Dedecek, Z. Sobalik and B. Wichterlova, *Top. Catal.*, 2004, **30–31**, 91–95.
44 L. Olsson and E. Fridell, *J. Catal.*, 2002, **210**, 340–353.
45 J. F. Moulder, W. F. Stickle, P. E. Sobol and K. D. Bomben, *Handbook of X-Ray Photoelectron Spectroscopy*, Perkin Elmer Corporation – Physical Electronics Division, Eden Prairie, 1992.
46 L. Vitos, A. V. Ruban, H. L. Skriver and J. Kollár, *Surf. Sci.*, 1998, **411**, 186–202.
47 A. Iglesias-Juez, A. B. Hungria, A. Martinez-Arias, A. Fuerte, M. Fernandez-Garcia, J. A. Anderson, J. C. Conesa and J. Soria, *J. Catal.*, 2003, **217**, 310–323.
48 A. Hellman and H. Grönbeck, *Phys. Rev. Lett.*, 2008, **100**, 116801.
49 D. Guo, Q. Guo, K. Zheng, E. G. Wang and X. Bao, *J. Phys. Chem. C*, 2007, **111**, 3981–3985.
50 A. Vojvodic, F. Calle-Vallejo, W. Guo, S. Wang, A. Toftelund, F. Studt, J. I. Martinez, J. Shen, I. C. Man, J. Rossmeisl, T. Bligaard, J. K. Norskov and F. Abild-Pedersen, *J. Chem. Phys.*, 2011, **134**, 244509–244508.
51 G. B. Ellison, G. E. Davico, V. M. Bierbaum and C. H. DePuy, *Int. J. Mass Spectrom. Ion Processes*, 1996, **156**, 109–131.
52 *CRC Handbook of Chemistry and Physics*, ed. D. R. Lide, CRC Press LLC, Boca Raton, 80th edn, 1999.
53 A. Keshavaraja, X. She and M. Flytzani-Stephanopoulos, *Appl. Catal., B*, 2000, **27**, L1–L9.
54 R. Burch, P. Fornasiero and T. C. Watling, *J. Catal.*, 1998, **176**, 204–214.
55 K. Arve, F. Klingstedt, K. Eränen, J. Wärnå, L. E. Lindfors and D. Y. Murzin, *Chem. Eng. J.*, 2005, **107**, 215–220.
56 A. Michaelides, Z. P. Liu, C. J. Zhang, A. Alavi, D. A. King and P. Hu, *J. Am. Chem. Soc.*, 2003, **125**, 3704–3705.